ASTRONOMY AND SPACE SCIENCE
www.csiro.au

Field structure at the focus of paraboloidal reflectors and comparison with ASKAP beams

David McConnell

ASKAP Commissioning and Early Science Memo 010
February 8, 2016

CSIRO Astronomy and Space Science
Cnr. Vimiera and Pembroke Roads
PO Box 76, Epping, NSW 1710, AUSTRALIA Telephone : +61 2 9372 4100
Fax : +61 2 9372 4310

Copyright and disclaimer

Important disclaimer

Contents

Summary

The measured dimensions of bore-sight beams formed by BETA (the Boolardy Engineering Test Array) are compared with those expected from a simple, symmetric electro-magnetic model of the ASKAP antennas. The total-intensity beams are found to have widths proportional to wavelength, but 8 - 10% wider than expected from the uniformly illuminated model. From this, an edge taper of -3.5dB is inferred for the illumination. Analysis of the polarized (XX and YY) beams leads to a more complex result, inconsistent with a single, frequency-independent illumination function. The total-intensity illumination function inferred from this analysis closely resembles that derived in memo ACES007 using a different method.

1 Introduction

When light from a point source is brought through a telescope to a focus, the distribution of intensity on the focal plane is dependent on the optics of the telescope. For a typical telescope with a circular aperture, that pattern of intensity (the point-spread-function, PSF) is close to the Airy pattern, which is the Fraunhofer diffraction pattern of a circular aperture. In practice the PSF will differ from the Airy pattern because of imperfections in the optics, because of the aperture being obstructed, because of the finite focal ratio, and from polarisation effects.

As a reference for measured beam dimensions, the Airy Pattern and the pattern in a model paraboloidal reflector are reviewed in sections §2 and §3. Section §4 compares these with measurements of holographic beam maps formed with ASKAP-BETA and its Mark I PAFs and beamformers. A brief discussion follows in §5.

2 The Airy pattern

The intensity of the Fraunhofer diffraction pattern of a circular aperture is called an Airy pattern (after G.B.Airy who described it in 1835). It is the squared modulus of the Fourier Transform of the circular aperture (see Born&Wolf). The intensity of light diffracted by a circular aperture of diameter $D = 2a$ onto a screen is

$$I(\theta) = I_0(\frac{2J_1(x)}{x})^2 \tag{2.1}$$

where J_1 is the Bessel function of the first kind of order one, $x = ka\sin\theta$, $k = 2\pi/\lambda$, and θ is the anglular measure of the pattern as viewed from the aperture.

Fig. 2.1 shows the Airy pattern, which has zeros at $x \simeq \pm 3.8317, \pm 7.0156, \pm 10.1735, ...$ For small θ, $x \simeq \pi\theta D/\lambda$; $x/\pi \simeq \theta D/\lambda$. Then the first zeros lie at $\theta \simeq \frac{\pm 3.8317}{\pi}\lambda/D \simeq \pm 1.22\lambda/D$. The height of the first sidelobe is $\sim 1.75\%$; it lies at $x \simeq 5.13562$, that is at $\theta \simeq 1.635\lambda/D$. The pattern falls to half its maximum at $x \simeq 1.6168$, so that the full width of the main lobe at half height (FWHM) is close to $\theta = 1.029\lambda/D$.

3 Fields in the focal plane of paraboloidal reflector

Minnett & Thomas (1968)—hereafter MT68—considered a circularly symmetric and perfectly conducting reflector as a model for a typical radio telescope. They consider a linearly polarised plane wave incident normally on the reflector and write the electric and magnetic fields $\mathbf{E}_s$, $\mathbf{H}_s$ scattered by a surface element dS of the reflector. By restricting the problem to regions close to the axis, these expessions are simplified to allow their integration over the whole reflector and so compute the total scattered field. The approximation made is equivalent to assuming that the scattered wavefront is planar over the axial region; the solution is restricted as

$$\rho/\lambda \leq 0.35\sqrt{r_0/\lambda}$$

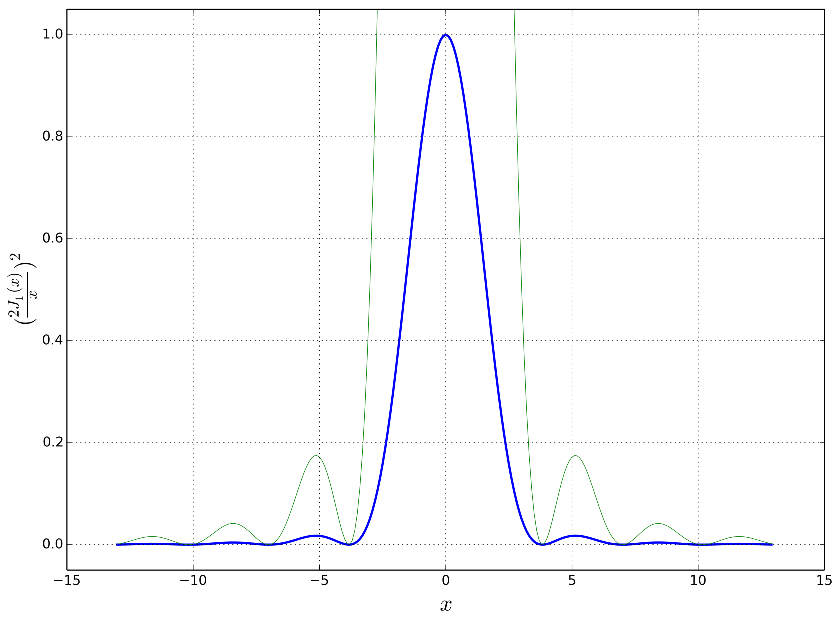

Figure 2.1: The Airy pattern as a function of $x = ka\sin\theta$, also shown with a x10 scale to highlight the sidelobes.

where ρ is the distance from the axis, and r_0 is the distance from reflector to the region being considered. For this region, MT68 express the total scattered field as integrals over the reflector surface, broken into a series of annular elements. They show that the total field in a transverse plane due to an annular ring is the sum of TE and TM (transverse electric and transverse magnetic) axial waves, propagating at the same velocity and so travelling as a "Hybrid axial wave". MT68 then apply the general description to the focal region of a paraboloidal reflector. Field descriptions are further simplified by confining the analysis to a small distance z from the focal plane ($z = 0$)

$$\frac{|z|}{\lambda} \leq \frac{0.35\sec^2\theta/2}{\sqrt{1+\cos^2\theta}}\sqrt{\frac{f}{\lambda}}$$

Here θ is the angular displacement of a surface element from the vertex as viewed from the focus; it ranges from 0 to θ_1 at the rim of the reflector[1]. For $f/D = 0.5$, $\theta_1 = 53.1°$. For the ASKAP antenna at 1 GHz ($\lambda = 0.3$m), the thickness of this zone is 3.4λ.

3.1 The focal plane distribution

MT68 give the components of the electric and magnetic fields in the focal plane referred to cylindrical polar coordinates $(\rho, \xi, z,)$, but use a generalised distance U from the axis

$$\begin{aligned} U &= k\rho\sin\theta_1 \\ k &= 2\pi/\lambda \end{aligned} \tag{3.1}$$

Here I give equations 33a, 33b and 34 from MT68.

$$\begin{aligned} E_\rho &= E_\rho(U)\sin\xi \\ E_\xi &= E_\xi(U)\cos\xi \\ E_z &= E_z(U)\sin\xi \end{aligned} \tag{3.2}$$

---

[1] MT68 use the symbol θ_0 for this quantity. The change here is made to allow for the discussion below in the §3.3 about the central blockage.

with corresponding terms for $\mathbf{H} = (H_\rho, H_\xi, H_z)$.

$$\begin{aligned} E_\rho(U) &= -2jkfE\sin^2\frac{\theta_1}{2}\{A(U)+B(U)\} \\ E_\xi(U) &= -2jkfE\sin^2\frac{\theta_1}{2}\{A(U)-B(U)\} \\ E_z(U) &= -8kfE\sin^2\frac{\theta_1}{2}\{C(U)\} \end{aligned} \tag{3.3}$$

$$\begin{aligned} A(U) &= \frac{1}{2}\mathrm{cosec}^2\frac{\theta_1}{2}\int_0^{\theta_1}\sin\theta J_0(k\rho\sin\theta)e^{jkz\cos\theta}d\theta \\ B(U) &= \frac{1}{2}\mathrm{cosec}^2\frac{\theta_1}{2}\int_0^{\theta_1}\sin\theta\tan^2\frac{\theta}{2}J_2(k\rho\sin\theta)e^{jkz\cos\theta}d\theta \\ C(U) &= \frac{1}{2}\mathrm{cosec}^2\frac{\theta_1}{2}\int_0^{\theta_1}\sin^2\frac{\theta}{2}J_1(k\rho\sin\theta)e^{jkz\cos\theta}d\theta \end{aligned} \tag{3.4}$$

Evaluation of these expressions yield the electric fields in the focal plane resulting from an incident wave polarised in the Y direction, that is where $\xi = \pi/2$. Fig. 3.2 shows the field distribution so computed, using $\theta_1 = 53.1^\circ$, corresponding to the focal ratio $f/D = 0.5$ of the ASKAP antennas. To prepare this plot the radial and tangential fields E_ρ, E_ξ were transformed to the horizontal and vertical E_X, E_Y. The figure shows the magnitude of the electric field as contours and its direction as vectors. Note that the pattern is not circularly symmetrical: the central lobe is elliptical as are the dark and bright bands that surround it; the dark and bright bands have 4- and 2-fold azimuthal symmetry respectively.

To allow comparison of the patterns described above with observed beam shapes, the generalised coordinate U describing distance on the focal plane must be transformed to angular units that can be measured on the sky. Two steps are necessary. First, a position on the focal plane that lies some distance from the axis can be described by the angle α_f that distance subtends from the reflector vertex. Second, to that angle α_f there corresponds an angular displacement α on the sky, the two angles being related by a so-called Beam Deviation Factor. Fig. 3.1 illustrates the geometry.

A displacement ρ on the focal plane that is small compared with the focal length f subtends an angle

$$\alpha_f \simeq \rho/f$$

Rearranging the expression 3.1 for U, and setting the focal ratio $F = f/D$ we then get

$$\begin{aligned} \alpha_f &= \frac{U}{\pi}\frac{\lambda}{2f}\frac{1}{\sin\theta_1} \\ &= H\frac{\lambda}{D}\frac{U}{\pi} \end{aligned} \tag{3.5}$$

$$\begin{aligned} H &= \frac{1}{2F}\frac{1}{\sin\theta_1} \\ &= \frac{16F^2+1}{16F^2} \end{aligned} \tag{3.6}$$

For ASKAP $F = 0.5$ and $H = 1.25$.

The Beam Deviation Factor depends upon the focal ratio and for ASKAP antennas BDF $\simeq 0.86$ (Reynolds 2014). Combining this with equation 3.5 we get

$$\alpha = 0.86 \times 1.25 \times \frac{\lambda}{D}\frac{U}{\pi} \tag{3.7}$$

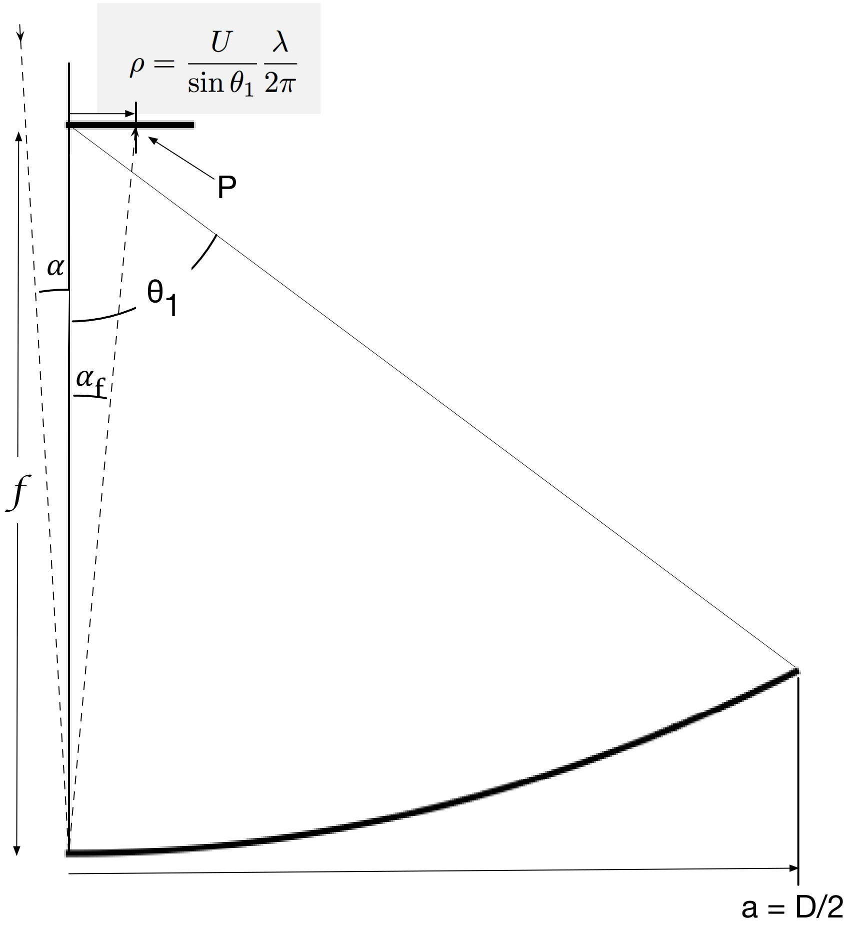

Figure 3.1: A diagram showing a parabolic antenna of semi-diameter a and focal length f. θ_1 is the angle from vertex to rim seen from the centre of the focal plane. The point P on the focal plane is displaced from the axis by ρ and has angular displacement α_f from the vertex. The source of radiation on the sky that focuses at P has angular displacement from the axis $\alpha =$ BDF $\times\, \alpha_f$.

3.2 Beam shapes

The form of the brightness distribution over the beam is computed simply as the square of the voltage pattern computed in the previous Section. Fig. 3.3 shows the X and Y beams; the ellipticity of the main lobe shape is clear, with the major axis aligned with the plane of polarisation. Fig. 3.4 shows both the total intensity beam, $XX+YY$, and the difference beam $XX-YY$, which for ASKAP antennas corresponds to Stokes U.

The sizes of the XX and YY beams, expressed as the full width at half maximum (FWHM) is $1.106\lambda/D$ and $1.061\lambda/D$ in the directions parallel and perpendicular to the incident polarisation. The total intensity beam, $XX+YY$, is symmetrical with FWHM $= 1.061\lambda/D$. Other parameters of the beams can be read off the profiles shown in Fig. 3.5.

3.3 Central blockage

The method used by MT68 can be easily adapted to account for a central blockage in the illumination pattern. The integrals in equation 3.4 can be calculated from θ_0 to θ_1, θ_0 lying at the edge of the shadow cast by the structure at the focus. For ASKAP antennas the central blockage has a diameter of 1.17 m giving $\theta_0 = 5.6°$. Recomputing the voltage and intensity patterns using the new limits of integration give only small changes to those computed without the central blockage. The full width at half maximum of

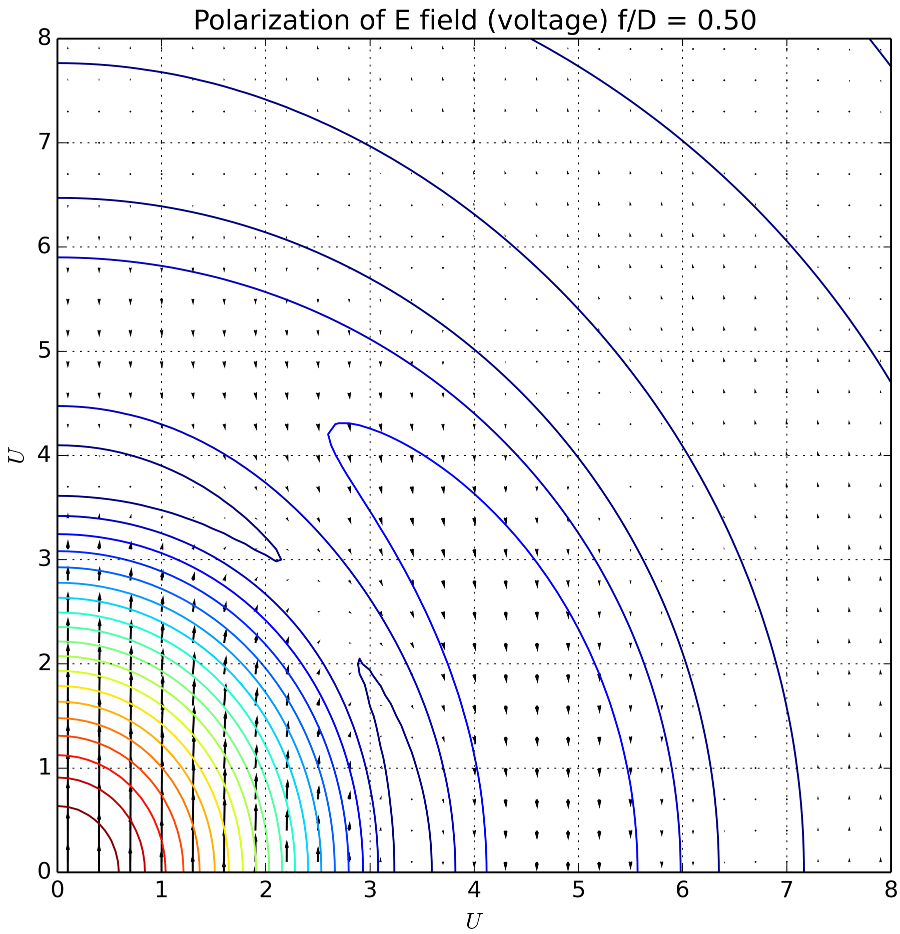

Figure 3.2: Field distribution in the focal plane of paraboloid with $f/D = 0.5$ ($\theta_1 = 53.1°$), in response to an incident wave polarised in the vertical (Y) direction. The contours are drawn at intervals of 5%; the arrows signify the field strength by their length and the field direction. Note the elliptical shape of the central lobe and the 180° reversal in the first side-lobe relative to the main lobe. This figure can be directly compared with Fig. 10 of MT68.

the total intensity beam decreases by 0.7%. The largest effect is in the height of the first sideload which increases from 2.7% to 3.2% of the main-lobe height.

3.4 Tapered illumination

The analysis above assumes the aperture is uniformly eliminated (with a central blockage in §3.3). In real telescopes, illumination is likely to be tapered, so that the outer parts of the reflector contribute less to the power collected at the focus. A function such as

$$T(\theta) = \cos(\frac{\theta}{\theta_t}\frac{\pi}{2}) \tag{3.8}$$

(which has a maximum on axis at $\theta = 0$, and falls smoothly to zero at $\theta = \theta_t$) can be used to describe the taper as it resembles the shape of the reception pattern of a typical receiving element (e.g. horn). A taper can be included in the formalism of MT68 by multiplying the integrand in equation 3.4 by the taper function T.

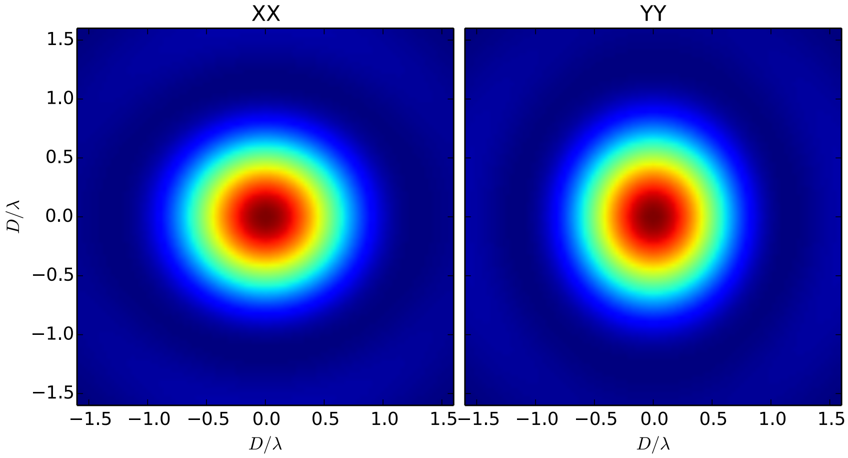

Figure 3.3: Diffraction pattern of a circular paraboloid with focal ratio $f/D = 0.5$. The Responses to the X and Y linearly polarised waves are shown in the left and right panels respectively. Note the elliptical shape of the main lobe, with major axis aligned with the plane of polarisation.

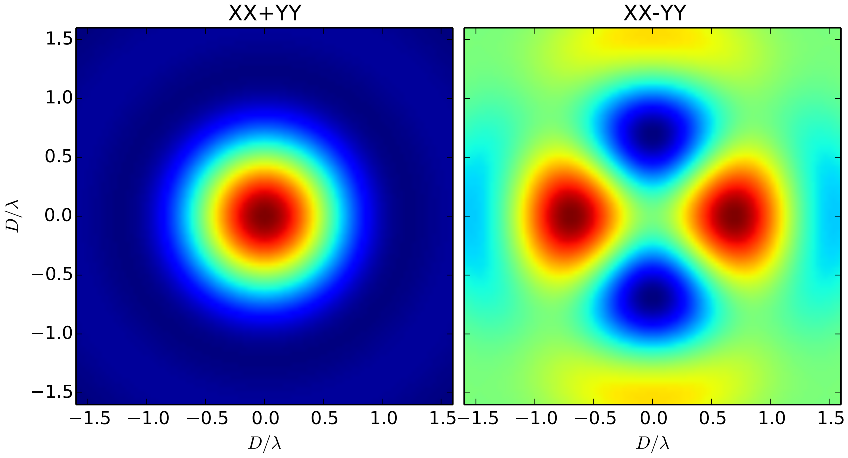

Figure 3.4: Diffraction pattern of a circular paraboloid with focal ratio $f/D = 0.5$. The left panel shows the sum of the X and Y polarised responses $XX + YY$. The right panel shows the difference $XX - YY$; this is the well-known clover-leaf pattern of off-axis instrumental polarisation.

3.5 Pattern summary

The dimensions of the Airy pattern and the patterns according to the MT68 model are summarised in Table 3.5.

4 Comparison with ASKAP beams

The shapes of formed beams on BETA have been measured using holography (Hotan 2016). These measurements usually cover an 8×8 degree area and are made for each of the 304 1-MHz channels. Figures 4.1 and 4.2 show the bore-sight beam formed on antenna AK15 with the beam weight file `201505120639_5872_9beams`, and measured in SBID 1803. The beam at 726 MHz is displayed. These figures can be compared directly with the computed patterns shown in Figures 3.3 and 3.4. The measured beam shapes have been rotated 45° relative to their normal display so that the polarisation axes X and Y are drawn horizontally and vertically as for all the intensity patterns displayed in §3 and by MT68. The measured beam shapes have been scaled by $\frac{\lambda}{D}$ to allow direct comparison with the computed

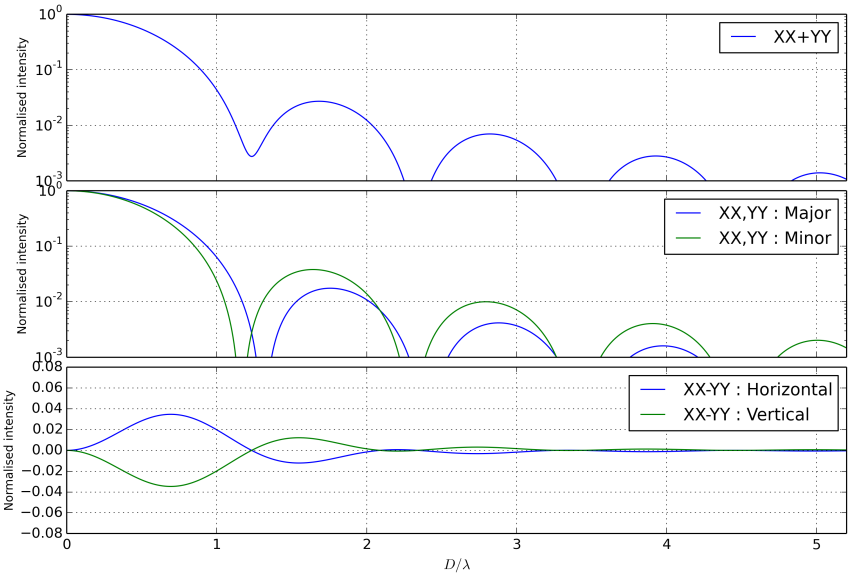

Figure 3.5: Profiles through the intensity distributions shown in Fig. 3.3 and 3.4. The top panel shows the radial profile through the symmetric total-intensity beam. The middle panel shows profiles through the elliptical XX and YY beams; the profile along the minor axis shows higher sidelobe levels. The bottom panel gives the vertical and horizontal profiles through the Stokes U beam ($XX - YY$); these can be related directly to the positive and negative lobes visible in the right-hand panel of Fig. 3.4.

	FWHM $\|,\perp$ (λ/D)	First null $\|,\perp$ (λ/D)	First sidelobe $\|,\perp$ (λ/D)	Sidelobe height $\|,\perp$ (%)
Airy	1.03	1.22	1.635	1.75
MT68 ($XX+YY$)	1.061	1.23	1.68	2.71
MT68 (XX,YY)	1.106,1.020	1.31,1.17	1.76 ,1.64	1.75 ,3.80
MT68,cb ($XX+YY$)	1.054	1.22	1.68	3.16
MT68,cb (XX,YY)	1.099,1.013	1.29,1.15	1.76 ,1.64	2.11 ,4.36

Table 3.1: Model patterns summarised by main lobe size, positions of the first null and sidelobe, and the height of the first side lobe. Where the patterns are not circularly symmetrical, two figures are given for the direction parallel $\|$ or perpendicular $\perp$ to the plane of polarisation.

intensity patterns.

The frequency of the beam displayed in Fig. 4.1 was chosen because of its strong resemblance with the computed patterns. Over the full frequency range there is considerable variation in the features of the measured beams, some showing marked deviations from the computed patterns. In the Sections below some of these differences are quantified.

4.1 Beam shape as an ellipse

Given the locus of the half-power contour as a set of points (x_i, y_i) it is possible to find the best (in a least squares sense) ellipse that fits those points. Pattern-recognition research has led to concise solutions to the problem; here I use the method and Python code provided by Nicky van Foreest[2]. The fitting routine returns the parameters of an ellipse from which we can calculate the position of centre, the position and angle of its major axis, and the lengths of the major and minor axes. These can be used in a quantitative assessment of the measured X, Y, and total intensity beams.

---

[2] http://nicky.vanforeest.com/misc/fitEllipse/fitEllipse.html

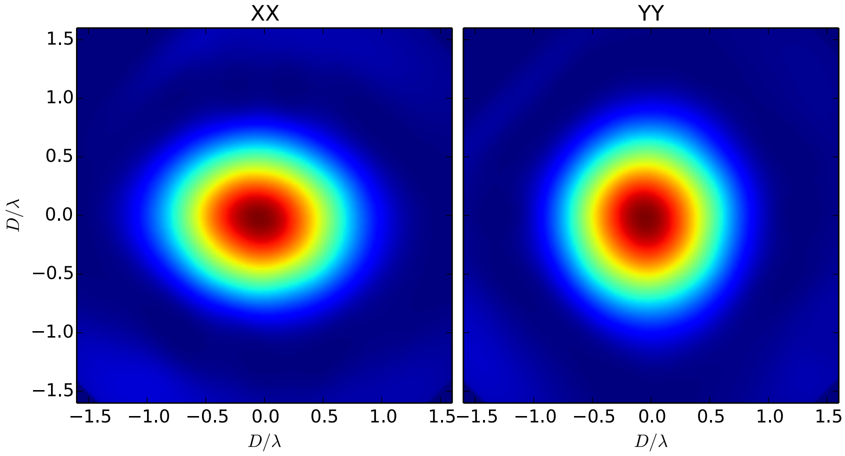

Figure 4.1: The intensity pattern measured across the bore-sight beam of antenna AK15 at 726 MHz. This beam was formed with the weights file `201505120639_5872_9beams`. Left and right panels show the XX and YY beams, rotated so that the X and Y planes of polarisation are displayed horizontally and vertically.

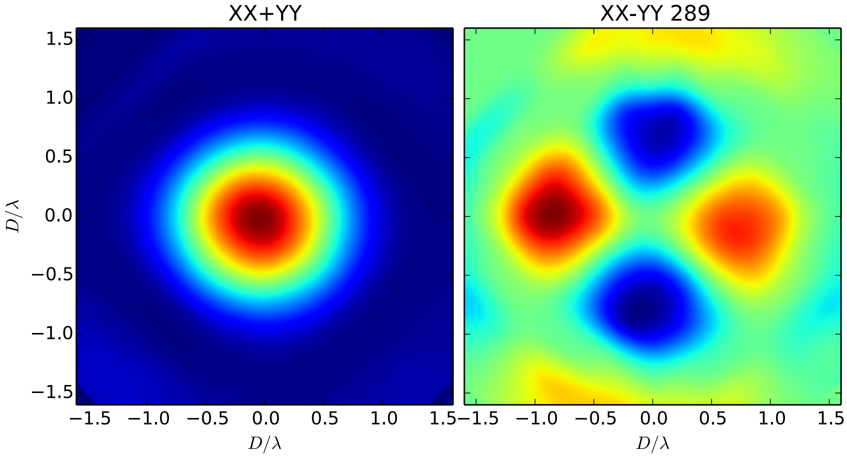

Figure 4.2: The intensity patterns of Fig. 4.1 but displayed as $XX + YY$ and $XX - YY$.

4.2 Measured beam size

Figures 4.3, 4.3 and 4.3 show the lengths of the major and minor axes of the half power ellipse for the measured total intensity, XX and YY beams as a function of frequency for all the measured antennas in SBID 1803. The size of the total intensity beams is approximately proportional to wavelength as expected, but the beams are significantly elliptical and larger than predicted by the MT68 model. The X and Y polarised beams are not proportional to wavelength in size, having an axial ratio that increases with wavelength.

4.3 Relative $X - Y$ beam positions

The beam pattern of the difference between the X and Y polarised responses (equivalent to Stokes U for ASKAP antennas), as illustrated in the right-hand panels of Figures 3.4 and 4.2, is sensitive to shape and position differences in the individual X and Y beams. In many cases the symmetry evident in the measured pattern shown in Fig. 4.2 is not present. Fig. 4.6 shows difference beams from a set of three frequency channels chosen to illustrate the effect of the X and Y beams having different positions. The examples in the left and right-hand panels show the effects of the X and Y beams being

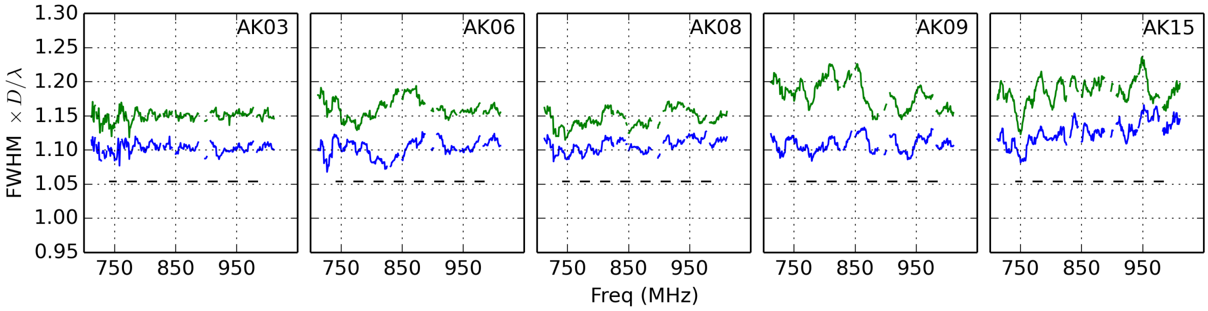

Figure 4.3: The lengths of the major and minor axes at the half power level of measured total intensity beams, as a function of frequency. The dashed line shows the value according to the MT68 model.

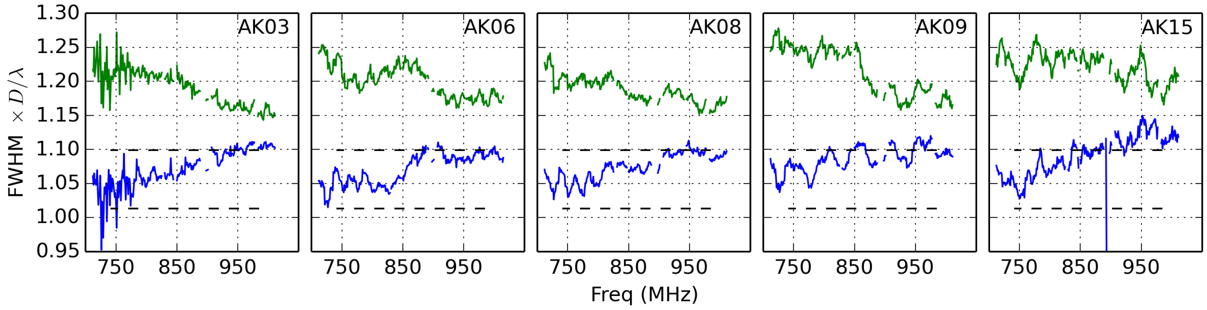

Figure 4.4: The lengths of the major and minor axes at the half power level of measured XX polarised beams, as a function of frequency. The dashed lines show the values for major and minor axis lengths according to the MT68 model.

displaced in the vertical and horizontal directions respectively. The example in the central panel has the symmetry expected of coincident X and Y beams. The range of relative displacements can be explored by looking at the centres of the half power ellipses used above for assessing beam size. For the three illustrated frequency channels, the positions of Y beam relative to X are, in (x, y) coordinates of the figures $(-0.004, -0.013)$,$(-0.005, -0.002)$ and $(-0.056, -0.002)\lambda/D$.

Fig. 4.7 shows, for each antenna measured, the relative displacements of the Y beam relative to the X beam. It can be seen that the antennas have different characteristics in this regard.

5 Discussion

It is common to refer to the diffraction pattern of telescopes as an Airy pattern, and the main lobe as an Airy disc. However, it is clear from §3 that the beam shapes of practical radio telescopes, with their relatively short focal ratios, depart significantly from the classic Airy pattern. The treatment of Minnett and Thomas summarised in §3 gives focal plane distributions for plane polarised waves that have elliptical main lobes and 4- and 2-fold azimuthal symmetry in the dark and bright bands surrounding them. This model is expected to differ from observed distributions: it takes no account of blockage from the tetrapod support and it assumes the central blockage to be circular.

A detailed matching of observed beam shapes with models derived from theory will involve many complexities beyond the scope of this note. The model itself is inadequate, at least for the reasons mentioned above and probably others. However, some physical insight may be gained from comparison of the broad features of the observed beams with this approximate model. In general, the beam shapes measured from BETA resemble the modelled distributions. The main differences are:

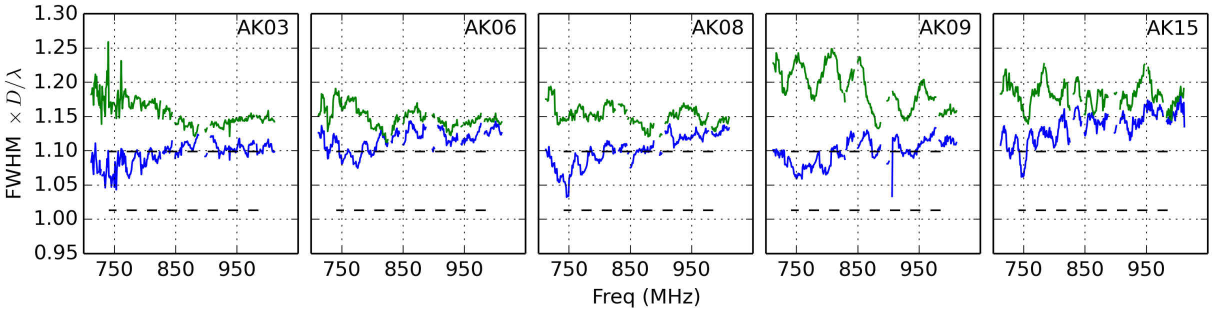

Figure 4.5: The lengths of the major and minor axes at the half power level of measured YY polarised beams, as a function of frequency. The dashed lines show the values for major and minor axis lengths according to the MT68 model.

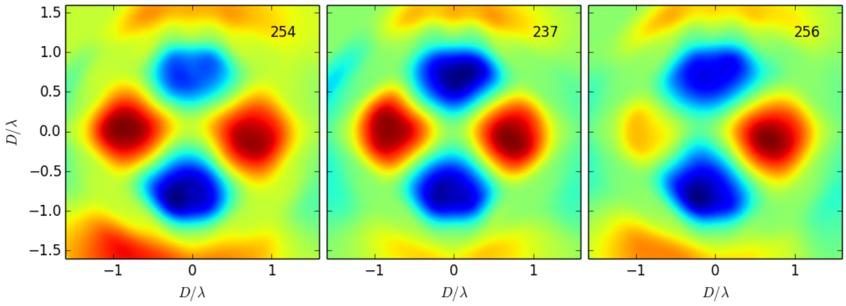

Figure 4.6: Differences of the measured X and Y polarised beams from antenna AK06 at three frequencies: 761, 778, and 759 MHz (channel numbers 254, 237, 256). Note the asymmetry between the negative (blue) lobes in the left-hand panel and between the positive lobes in the panel on the right.

- the size of the total intensity main lobes are about 5-10% greater than those in the model;
- the XX and YY polarised beams have major and minor axis lengths that are not strictly proportional to wavelength, and their axial ratios are wavelength-dependent;
- the measured beam sizes have an overall trend, with added random and systematic variations including pronounced periodicities;
- the beam positions are not always on axis, with position differences between the polarizations frequently observed.

The measured beams were formed using the maximum signal-to-noise ratio (MaxSNR) method. This method gives high weight to PAF elements in the brighter parts of the focused pattern. But it also down-weights elements that have low gain or high noise, wherever they fall in the pattern. Therefore, although the field distribution on the PAF may be well modelled by MT68, the actual beam formed will depend upon the individual characteristics of the elements in the PAF.

The total intensity beams have a main lobe with a low ellipticity and a size proportional to wavelength, but about 5-10% larger than expected from an MT68 model assuming uniform illumination (see Fig. 4.3). Fig. 5.1 shows the broadening expected for a range of illumination tapering as a function of θ_t in equation 3.8. It is assumed that this tapering results from the shape of the radiation (reception) patterns of the individual PAF elements. It is probably an oversimplification to assume an azimuthal symmetry in these patterns, and some ellipticity in the patterns may account for the departures from the expected axial ratios in the polarised beams. Glossing over these details, from Fig. 5.1 we can estimate a value of θ_t that leads to the observed broadening of the total intensity beams relative to their model widths: $\theta_t \simeq 75^\circ$. This corresponds to an edge taper of about -3.5 dB (a factor of 0.44). Illumination tapering is an

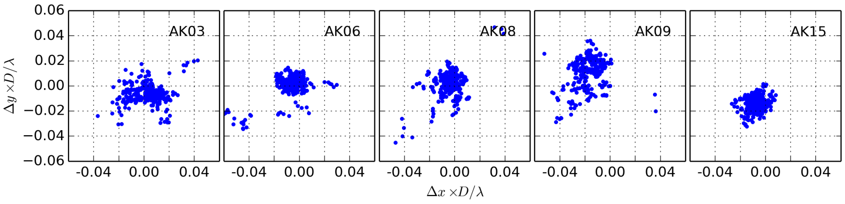

Figure 4.7: Positions of the Y polarised beams relative to the X across the 304 channel spectrum for each antenna. The position differences are in angular units of λ/D.

important contributor to the aperture efficiency of the antenna and it is interesting to note that the degree of tapering inferred here leads to an aperture efficiency of about 70%, similar to the value reported elsewhere (McConnell et al. 2015) from independent measurements.

5.1 Consistency with memo ACES007

In his assessment of the wide-field polarimetric potential for ASKAP, Bob Sault (Sault 2015) assessed the frequency-dependence of beam shape using a different technique. A single observation of B1934−638 was made with a square footprint with a 1.24° pitch. The source was at the centre of the boresight beam, but offset by 1.24° or 1.75° in the other eight. The results were fit to a beam model derived from the analysis of Ghobrial (1976), and were found consistent with the model illumination pattern with 44% taper at the dish edge. This is in excellent agreement with the tapering determined above. Note that the analysis described here is of just the bore-sight beam, whereas Bob Sault's analysis probes different points in all nine beams. The two approaches lead to the same inferred tapering function.

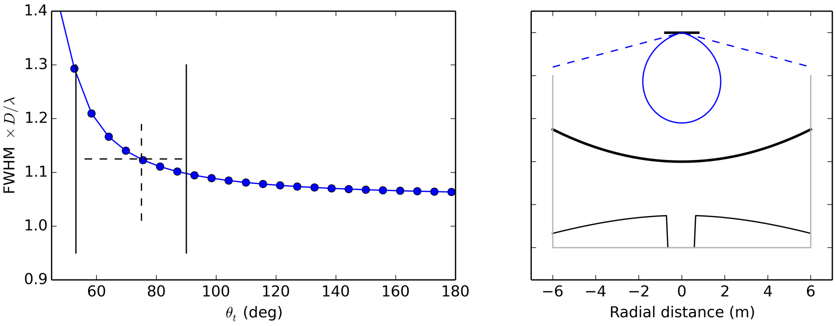

Figure 5.1: The left-hand panel shows the variation of main lobe width with the degree of illumination tapering. The form of the tapering used is that described in equation 3.8. θ_t is the angle at which the illumination function falls to zero. The two vertical lines correspond to the rim of the ASKAP dish ($\theta_t = \theta_1$) and 90°. The horizontal dashed line marks the approximate beam width observed with holography (see Fig. 4.3); and the vertical dashed line marks the value of θ_t corresponding to that width: $\theta_t \simeq 75°$. The right-hand panel is a schematic showing the reflector surface and the PAF in its focal plane. The blue dashed lines have an opening angle of $2\theta_t$. The curve at the bottom of the diagram shows the variation of illumination with distance across the reflector.

References

Ghobrial, S. I. 1976, Antennas and Propagation

Hotan, A. W. 2016, ACES memorandum, 11, 1

McConnell, D., Hotan, A. W., & Bannister, K. W. 2015, ACES memorandum, 5, 1

Minnett, H. C., & Thomas, B. M. 1968, Proc. Instn. Electr. Eng., 115, 1419

Reynolds, J. E. 2014, ACES memorandum, 1

Sault, R. J. 2015, ACES memorandum, 7, 1

CONTACT US

t 1300 363 400
+61 3 9545 2176
e enquiries@csiro.au
w www.csiro.au

FOR FURTHER INFORMATION

CSIRO Astronomy and Space Science
David McConnell
t +61 2 9372 4132
e David.McConnell@csiro.au
w Astronomy and Space Science